Review Article

Huygens HASI servo accelerometer: A review and lessons learned

B. Hathi [a,*], A.J. Ball [a,f], G. Colombatti [b], F. Ferri [b], M.R. Leese [a], M.C. Towner [a,e], P. Withers [d], M. Fulchigioni [c], J.C. Zarnecki [a]

[a] PSSRI–The Open University, Walton Hall, Milton Keynes, MK7 6AA, United Kingdom
[b] CISAS "G.Colombo"–Universita di Padova, Via Venezia, 1 35131 Padova, Italy
[c] Université Paris 7–LESIA, Observatoire de Paris-Meudon, 5 place Jules Janssen, 92190 Meudon, France
[d] Center for Space Physics, Boston University, 725 Commonwealth Avenue, Boston, MA 02215, USA
[e] Impacts & Astromaterials Research Centre (IARC), Department of Earth Science and Engineering, Imperial College London, South Kensington Campus, London, SW7 2AZ, United Kingdom
[f] ESA ESTEC, Noordwijk, The Netherlands

ARTICLE INFO

ABSTRACT

The servo accelerometer constituted a vital part of the Huygens Atmospheric Structure Instrument (HASI): flown aboard the Huygens probe, it operated successfully during the probe's entry, descent, and landing on Titan, on 14th January 2005. This paper reviews the Servo accelerometer, starting from its development/assembly in the mid-1990s, to monitoring its technical performance through its seven-year long in-flight (or cruise) journey, and finally its performance in measuring acceleration (or deceleration) upon encountering Titan's atmosphere.

The aim of this article is to review the design, ground tests, in-flight tests and operational performance of the Huygens servo accelerometer. Techniques used for data analysis and lessons learned that may be useful for accelerometry payloads on future planetary missions are also addressed.

The main finding of this review is that the conventional approach of having multiple channels to cover a very broad measurement range: from $10^{-6}g$ to the order of $10g$ (where g = Earth's surface gravity, $9.8\,\mathrm{m/s^2}$), with on-board software deciding which of the channels to telemeter depending on the magnitude of the measured acceleration, works well. However, improvements in understanding the potential effects of the sensor drifts and ageing on the measurements can be achieved in future missions by monitoring the 'scale factor'—a measure of such sensors' sensitivity, along with the already implemented monitoring of the sensor's offset during the in-flight phase.

© 2009 Elsevier Ltd. All rights reserved.

Contents

---

* Corresponding author. Tel.: +44 1908 659 593; fax: +44 1908 858 022.
  E-mail address: b.hathi@open.ac.uk (B. Hathi).

1. Introduction

Accelerometers have been included in payloads since the early days of Earth re-entry modules (Seiff, 1963; Peterson, 1965a); therefore, it is of little wonder that all planetary probes continue to have some form of accelerometry payloads. Their popularity stems from their wide-ranging applications: from triggering critical spacecraft events during entry and descent, to inferring various planetary properties. The Huygens mission to Titan (Lebreton et al., 2005) consisted of a probe equipped with various science instruments to study Titan and its atmosphere (Lebreton and Matson, 2002), and broadly two groups of accelerometers. The first group, the system accelerometers, consisted of the Radial Acceleration Sensor Unit (RASU) and the Central Acceleration Sensor Unit (CASU), whose main tasks were to measure the spin rate during the probe's descent and to trigger key mission sequence events, respectively (Jones and Giovagnoli, 1997; Clausen et al., 2002). The second group, the science accelerometers, were distributed between two of Huygens' six scientific instruments: the Huygens Atmospheric Structure Instrument (HASI) and the Surface Science Package (SSP). This paper focuses on a highly sensitive accelerometer, henceforth referred to as 'the Servo', which was included as a sub-system in the HASI instrument suite and whose main task was to infer Titan's upper atmosphere density profile.

There are several references describing the HASI instrument in its entirety (Fulchignoni et al., 1997, 2002); in summary, the accelerometer sub-system consisted of three orthogonally mounted piezo-resistive (PZR) accelerometers and the Servo,

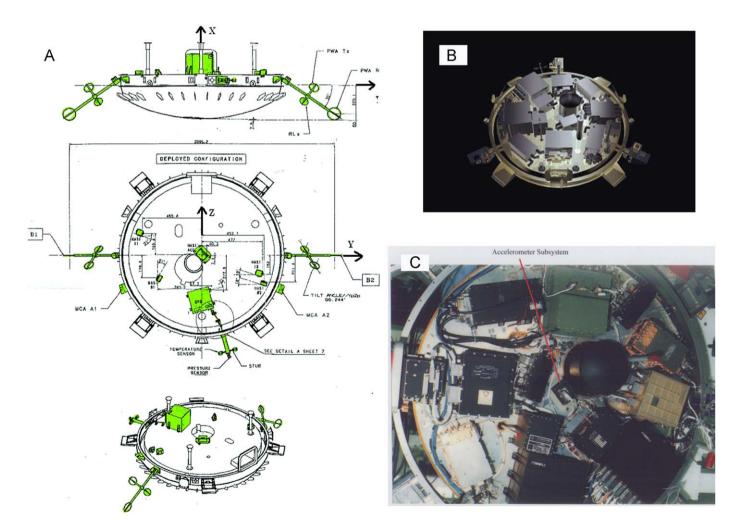**Fig. 1.** Shows the central location of the accelerometer sub-system unit, containing the Servo, from the technical drawing perspective (A), the computer-aided-design CAD (B), and the photograph (C). The HASI Servo is located as close to the Huygens probe's centre of mass (CM) as possible; its location relative to the CM, in the probe's reference frame [X, Y, Z], is [−6.00, 14.65, 1.42] mm (Colombatti et al., 2008b).

Specifications

Performance
- Input range ±60 g
- Bias <4 mg
- Scale factor 1.33 mA/g ±10%
- Axis misalignment <2 mrad
- Resolution/Threshold <1 µg
- Bandwidth >300 Hz

Environmental
- Operating temperature range -55 to +95°C
- Shock 250 g
- Vibration 15g, peak sine, 20-2000Hz

Electrical
- Input voltage ±13 to ±18 VDC
- Quiescent current <16 mA per supply
- Quiescent power <480 mW @ ±15 VDC

Physical
- Weight 71 grams
- Size 1.0 in. dia. X 0.96 in. high
- Case material Stainless steel

Fig. 2. The Servo sensor (QA2000, Q-Flex accelerometer), along with its main properties. The right-hand section of the image shows the schematic representation of the Servo unit. The voltage across resistor R_L gives a measure of the acceleration; R_L also determines the device's sensitivity in terms of volts per unit acceleration (V/g). The device has an inbuilt temperature sensor.

mounted along the probe's descent axis to measure acceleration (or more accurately, deceleration). The aim of the PZR was to detect the impact at landing, hence its operating range was 0–2000g (where g = Earth's surface gravity, 9.8 m/s^2), giving a rather coarse accuracy of $\pm 0.4\,g$ (Fulchignoni et al., 2002). The primary aim of the Servo was to determine Titan's atmospheric density profile during the probe's high-speed entry (i.e. supersonic and above) phase. The pressure and temperature profiles can be inferred from the density profile and by using equations of hydrostatic equilibrium and state, respectively (see outputs in Fig. 13). Fig. 1 shows the location of the accelerometer sub-system unit (containing the Servo) on the Huygens probe.

2. Building blocks of the Servo unit

2.1. The sensor

The main component of the Servo unit was its highly sensitive Q-Flex accelerometer shown in Fig. 2, which was at the time (~1992) procured from Sundstrand, and is now be available through Honeywell Inc (more details from http://www.inertialsensor.com). The sensor works on the principle of 'servo electronics',[1] where the current required to return a small proof mass to its null position, along a single axis, is proportional to the input acceleration.

---

[1] The Electronics Handbook (1996) quotes: "A servo system is defined as a combination of elements for the control of a source of power in which the output of the system, or some function of the output, is fed back for comparison with the input and the difference between these quantities is used in controlling the power (James et al., 1947)".

2.2. Signal conditioning electronics

The signal conditioning circuitry, shown in Fig. 3, was kept to a minimum in order to reduce the chances of component failures during their seven-year-long exposure to the space environment (i.e. radiation and vacuum) during cruise. The total resistance across the Servo's output, from a combination of two load resistors, determines its measurement range (either ±20 mg (or milli-g) or ±18.5 g). The output voltage, taken across a load resistor combination, is made available as two channels: unamplified (unit gain) and ×10 amplified. Hence the total number of Servo measurement ranges available, following amplification and ±10 V A/D (12-bit) conversion, are: (1) ±2 mg, (2) ±20 mg, (3) ±1.85 g, and (4) ±18.5 g (Zarnecki et al., 2004).

2.3. Software

The on-board Servo software had two functions: (1) to select the Servo's measurement range (by switching between load resistors), dependent on the magnitude of deceleration experienced by the probe and (2) to reduce and package data for telemetry down-link, according to available bandwidth during different phases of the mission. The software functions are summarised in Fig. 4: while the 'Resolution' setting is time-driven, the software is able to switch back at any time, if the output drops to 10% (or increases to 90%) of the full scale.

2.4. Lessons learned

The above implementation of four measurement ranges and the associated software is a well-rehearsed route; albeit in some
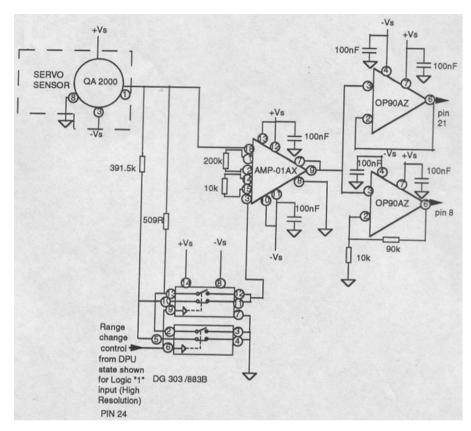
Fig. 3. The front-end signal conditioning electronics for the Servo unit. The output from the Servo 'sees' one of the two load resistors, depending on the bit set by the HASI Data Processing Unit (DPU). Either, the load resistance is set to 509 Ω (i.e. the low resolution, ±18 g scale), or 391.5 kΩ (the high resolution, ±0.02 g (or 20 mg) scale). The output is made available at two gain levels: $\times10$ gain (pin 8 on the right hand side) and $\times1$ gain (pin 21). Both output channels (i.e. pins 8 and 21) are sampled (individually) at 400 Hz by a 12-bit ADC whose full-scale range is ±10 V.
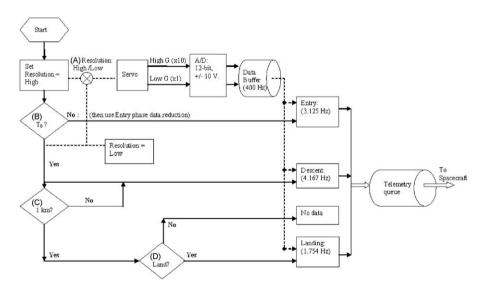

Fig. 4. The main functions of the Servo's on-board software. *Notes*: (1) The T_0 time/event indicates the start of the descent sequence (Lebreton et al., 2005) and occurs when the probe's housekeeping accelerometer detects the atmosphere. (2) The decision points (B), (C) and (D) also have a backup timeout value. (3) Data are reduced by taking every fourth value from the data buffer (i.e. 100 Hz), followed by summing and averaging variable number of samples depending on the mission phase (e.g. 32 samples in Entry phase results in 3.125 Hz effective sample rate) event.

varying form, this method has been implemented on the two Vikings (NASA-TN-3770218, 1976), Pathfinder (Seiff et al., 1997; Magalhães, 1999), and Galileo (Seiff and Knight, 1992) probes. Given such a strong and successful heritage, and now with the addition of the Huygens probe, the overall design philosophy is hard to fault. Except, in this particular implementation the in-

flight test capability of the Servo's scale factor ('*sf*' in Eq. (2)), a measure of the Servo's 'acceleration sensing' capability, was omitted. There is an option available on the Servo to stimulate the sensor, by allowing a known current to pass through the sensor's inputs, and measure the resulting output (see Fig. 2 'current self-test' pin 2 on the schematic, (Q-Flex Accelerometer

Handbook, 1997; Cardy, 1984)). If this self-test had been implemented, then any deviation in Servo's scale factor from its pre-launch value would have been better characterised, leading to a more accurate determination of the deceleration magnitudes at Titan. The most likely reason for not implementing the scale factor self-test/calibration may have been to retain simplicity in the circuit design, thereby reducing the probability of failures.

3. Assembly, integration, and pre-launch tests

3.1. Location on the probe

Since one of the goals of the Servo was to detect Titan's atmosphere by measuring the aerodynamic deceleration along the probe's descent axis, it was desirable to keep contributions from other motions (such as spin) to a minimum. The Servo unit was therefore mounted as close as possible to the probe's centre of mass (CM). The details of the Servo's mounting position relative to the CM can be found in Colombatti et al. (2008b). It is important to note that during the entry and descent phases, the probe's CM position changes as the probe's entry modules and parachute are ejected. During entry, the front shield suffers ablation and the heat resistant blanket (covering the shield) burns off. The modelled change in the probe's overall mass as a function of time is shown in Fig. 5.

The (non-aerodynamic) acceleration term, a_w, arising from the CM-Servo position offset (in Eq. (1)) (Cancro et al., 1998.), needs to be removed from the measured acceleration before calculating the density profile. a_w is a function of the distance between probe's CM and the Servo, r, the angular rate of the probe, w, and the angular acceleration of the probe, α.

$$\overline{a}_w = \overline{w} \times (\overline{w} \times \overline{r}) + \overline{\alpha} \times \overline{r} \tag{1}$$

Note: all terms: a_w, w, r and α are vectors.

3.2. Ground tests

The testing philosophy on the Huygens mission was to run a standard, time-line driven, mission execution sequence following integration of each instrument on the probe platform. The post instrument-probe integration testing was extensive, covering various environmental (thermal vacuum, electromagnetic compatibility and vibration) tests. Additionally, a test was carried out to characterise the alignment of Servo-to-probe axes. The test involved rotating the probe on a frame in 1-degree steps and recording Servo outputs at each step.

3.3. Lessons learned

The test programme, with the usual European Space Agency's reviews, was comprehensive—no further tests need to be added by future instruments.

If the mass, power and data budgets allow, then a better option would be to consider having two sets of 3-axis Servo sensors, mounted 180° apart on the probe's platform along the axis in which the probe's CM is projected to change the most. This arrangement gives six degrees of freedom, allowing a better determination of the probe's nutation/coning motion.

Another important lesson is to get an arrangement in place, as early as possible, between the prime contractor and the project management to characterise the drag coefficient as a function of various aerodynamic parameters. The uncertainty in drag coefficient constitutes a major source of error in constructing atmospheric profiles (Peterson, 1965a). In simulating extreme cases of the Huygens descent, (Kazeminejad et al., 2004) used $\pm 5\%$ error around the drag coefficient data set. Fig. 6 shows the drag coefficient values used for Huygens analysis after using the available aerodynamic database and a few iterations (Kazeminejad et al., 2007).

4. Post-launch (cruise) checkouts: data analysis

One of the objectives of the post-launch (also known as 'in-flight' or 'cruise') checkout campaign was to check the functionality of all instruments aboard the Huygens probe. A total of 16 in-flight checkouts, F1–F16, were carried out during the cruise
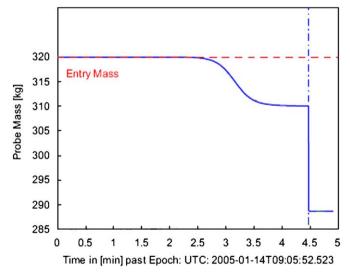
Fig. 5. Huygens mass evolution during entry was modelled by (Gaborit, 2004) and used in reconstructing the atmospheric profiles as described in Kazeminejad et al. (2007) and Colombatti et al. (2008a). The probe's centre of gravity (CoG) position, in the [X,Y,Z] frame, at the start and end of the entry phase is quoted in Lebleu et al. (2005) as: [75.44, 1.75, 5.38] and [82.54, 2.48, 5.13] mm, respectively. The CoG position, together with the initial CM offset (quoted under Fig. 1), may be used to work out the end of entry phase CM offset.

Fig. 6. Variations in the drag coefficient values as a function of altitude were 'iteratively refined' as described in Kazeminejad et al. (2007). In summary, the drag coefficient values are initially chosen by interpolating the Huygens aerodynamic database and used to calculate the atmospheric profiles, particularly the density (ρ) and the temperature (T) profiles. The ρ, T, and, and velocity profiles are used to improve the estimates of Mach and Knudsen numbers, which in turn are used to improve the drag coefficient. A similar method (of iteratively refining the drag coefficient) was used in analysing accelerometry results from Mars Pathfinder (Magalhães et al., 1999)

phase. The checkouts: starting from 8 days after launch (F1), were roughly spaced at six monthly intervals until the Titan encounter (F16). The Servo data from the freefall, zero-g, state, as provided by the cruise environment proved a valuable source in understanding the Servo and the noise present in this particular circuit configuration.

To convert acceleration measurements from raw units (in Volts) to units of acceleration (in $\mathrm{m\,s^{-2}}$), the following relationship is used:

$$a(\mathrm{m\,s^{-2}}) = \left(\frac{1}{sf(\mathrm{A/m\,s^{-2}})} \cdot \frac{a(\mathrm{V})}{R_L(\Omega)}\right) - offset\ (\mathrm{m\,s^{-2}}) \qquad (2)$$

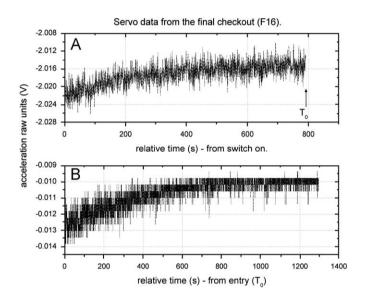where sf is the scale factor and R_L the load resistor.

Fig. 7. Typical Servo (raw) data from cruise checkouts; this data set is from the final (F16) checkout and is essentially a measure of the zero-g acceleration offset. Although the HASI Servo had 4 measurement ranges: (1) $\pm 2\,\mathrm{mg}$ (milli-g), (2) $\pm 20\,\mathrm{mg}$, (3) $\pm 1.85\,\mathrm{g}$, and (4) $\pm 18.5\,\mathrm{g}$, the data were mainly available from only two ranges, due to the steady, zero-g acceleration plus some (random and thermal) noise. Fig. 7(A) shows the high-resolution, 15 min, raw data (from the $\pm 2\,\mathrm{mg}$ range); Fig. 7 (B) shows the low-resolution data (from the $\pm 1.85\,\mathrm{g}$ range).

See Appendix A 'converting servo data to acceleration (in $\mathrm{m\,s^{-2}}$) from manufacture's data'.

Eq. (2) shows the linear relationship (of the form: $y = mx + c$) between raw acceleration, $a(\mathrm{V})$, and converted acceleration, $a(\mathrm{m\,s^{-2}})$. The *offset* is close to zero; its exact value depends on the Servo's input current (as set by resistor R_L in Fig. 2) and the operating temperature. The *scale factor* determines the Servo's sensitivity in terms of Amps/g (or Amps/$\mathrm{m\,s^{-2}}$); it is specific to a sensor and also varies with the operating temperature. Appendix A gives manufacturer's calibration of these two parameters for the specific Servo sensor flown on Huygens. The succeeding analysis outlines the observations made from the analysis of the Servo's output, in terms of noise/drifts and its implications on the *offset* values.

4.1. Cruise-checkout (raw) data

During each checkout, the Servo operated on a descent time-line simulating Huygens entry into Titan's atmosphere. Therefore, the data consists of same sequence: approximately 15 min of high resolution, pre-entry data, where thin atmosphere needs to be detected, followed by two hours of low-resolution data. Fig. 7 shows a typical cruise data set; this is from the final checkout, F16, carried out approximately one month before Huygens–Cassini separation on 25th December 2004.

4.2. Noise measurements from cruise-checkout data

While it is not possible to monitor changes in the scale factor (sf in Eq. (2)) from manufacturer's calibration, the cruise conditions are ideal for tracking drifts in the offset. Fig. 7(A) shows a trend in the zero-g offset that appears to rise over time; this is due to thermal drift within the Servo. Superimposed with the thermal drift is an oscillating signal, whose standard deviation (the 1-sigma scatter) may be obtained after removing the drift: i.e. by subtracting a 7-point median value from the original signal, or with respect to a 3rd order polynomial fit as described in Zarnecki et al. (2004). The 1-sigma noise values associated with the oscillations from each of the cruise checkouts, F1–F12, were presented in Zarnecki et al. (2004); an update is given here in Table 1.

Table 1
1-sigma noise values from checkouts—F1–F16.

Cruise checkout no.	Noise (1σ)		Temperature range (K)	Duration (min)	Date	Heliocentric distance (AU)
	(V)	(µg)				
F1	0.0014	0.3	288.3/291.8	14.9	23/10/1997	1.0
F2	0.0015	0.3	287.6/289.6	8.0	27/03/1998	0.7
F3	0.0015	0.3	284.7/288.2	15.0	27/12/1998	1.6
F4	0.0016	0.3	285.8/289.0	13.7	15/09/1999	1.3
F5	0.0015	0.3	283.8/287.3	15.0	03/02/2000	2.9
F6	0.0070	1.4	285.1/288.3	13.7	28/07/2000	4.1
F7	0.0071	1.4	286.1/289.5	14.9	22/03/2001	5.5
F8	0.0016	0.3	284.4/287.6	13.7	20/09/2001	6.4
F9	0.0016	0.3	282.1/285.6	14.9	17/04/2002	7.2
F10	0.0016	0.3	281.6/284.9	13.7	16/09/2002	7.7
F11	0.0013[a]	0.2	283.7/285.8	14.0	30/04/2003	8.2
F12	0.0016	0.3	281.1/284.2	12.8	18/09/2003	8.6
F13	0.0037[b]	0.7	289.4/290.4	5.8	20/03/2004	8.9
F14	0.0016	0.3	283.5/287.1	14.2	14/07/2004	9.0
F15	0.0016	0.3	282.0/285.0	12.8	14/09/2004	9.0
F16	0.0016	0.3	281.8/284.9	12.8	23/11/2004	9.0

[a] F11 had missing telemetry that probably lead to a slight under estimation of the noise.
[b] F13 had instrument-specific telecommanding activities, leading to a shorter test duration and higher-than-average noise.
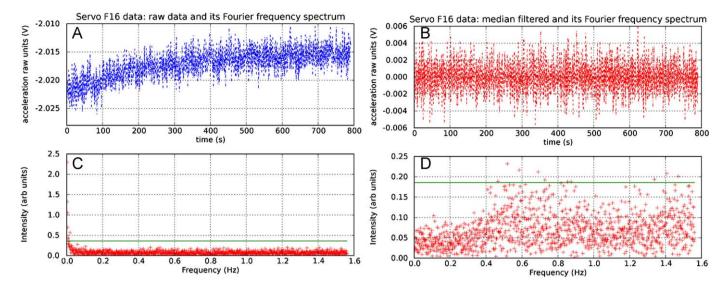
Fig. 8. Fourier analysis of the high-resolution data from F16. (A): Raw Servo data (same as Fig. 7(A)). (B): flattened (or median filtered) data; after subtracting a 7-point moving median average from data in (A). (C) and (D) are frequency spectra of raw and median filtered data respectively. The horizontal line in (C) and (D) gives the 'mean+3·σ' threshold; frequency components above the threshold line are referred in the text as 'dominant components'. While the temperature trend appearing in the raw spectrum in (C) around 0 Hz masks other components, the filtered data in (D) show some components above the threshold.

From Table 1, we notice that the 1-sigma noise for checkouts F6 and F7 are significantly higher at 1.4 μg, than the typical 0.3 μg level seen in most other checkouts. In order to see if there is any periodicity present in the higher noise data, we compare frequency spectra from F6 and F7 with a 'typical' data set F16. The dominant frequency components are obtained by first removing the drift (i.e. by subtracting a 7-point median value from the original signal), followed by running a Fourier transform. Fig. 8 shows the steps involved in processing data from the last checkout, F16, and its noise frequency spectrum.

Running Fourier transforms on the two data sets (see Fig. 9) show some dominant frequency components around the 0.4 Hz region (and its multiples) in F6, while the F7 shows a strong presence of oscillations at 1 Hz (in intensity terms, the 1 Hz component is greater than the temperature trend that appears around the 0 Hz region). These two checkouts were on either side of the Cassini–Huygens spacecraft's closest flyby past Jupiter (30th December 2000). There was also a problem, occurring around the same time as the closest flyby, with one of the four reaction wheels experiencing more friction. Since only three reaction wheels are required to control the spacecraft's attitude, the reaction wheel with friction problem was made redundant. During the interim period, the spacecraft was controlled by its 'hydrazine thruster attitude control system' as reported in Hansen et al. (2004). Further conclusions from the Servo observations presented in Fig. 9 are only possible if the spacecraft's navigation data were to be correlated with the Servo data—a task still outstanding at the time of writing this article.

The high-resolution data (up to ±2 mg) plotted over several checkouts, show movement in the zero-g offset over the duration of the Cassini–Huygens cruise phase (from 1997 to 2004) as shown in Fig. 10. Since the offset values are in m s⁻² (see Eq. (2)), any discrepancy between the perceived and the actual offset values (see Appendix A: 'offset values'), may translate into a systematic error on acceleration measurements. Hence, the error due to offset may be particularly significant for small-magnitude acceleration measurements.

If we convert the raw data in Fig. 7 to acceleration (in m s⁻²) using values in Appendix A, we see a step-change in the cruise offset values (see Fig. 11) when the Servo switches from the highest resolution (measuring ±2 mg) to a coarser resolution

(±1.85 g). Clearly the cruise environment must yield a constant acceleration (around 0 m s⁻² given that the spacecraft is in a 'freefall' state), so this anomaly in converting data needs to be explained. On examination of Eq. (2) (or Eq. (A1) from Appendix A) and the circuit in Fig. 2, it becomes clear that the current method of handling the offset does not take into account the effect of Servo's feedback load resistance on the offset. The offset is a function of: (1) Servo's acceleration measurement range (as set by load resistor R_L in Fig. 2) and (2) the drifts due to temperature and ageing effects (as seen in Fig. 10).

For the two most widely tested scenarios in cruise checkouts, namely the high-resolution entry (which delivers Servo data through the 'high-gain, high-resolution' load, as set out in Table A1, in Appendix A) and the low-resolution (±1.85 g) descent data, an alternative form of equation Eq. 2 may be used. This alternative form (i.e. Eq. (3)) uses the offset measurements (offset(V)) from a preceding checkout to subtract an appropriate level of offset for a particular resolution setting, as well correct any offsets drifts that may have occurred in the cruise phase.

$$a(\text{m s}^{-2}) = \left(\frac{1}{sf(\text{A/m s}^{-2})} \cdot \frac{a(V) - offset(V)}{R_L(\Omega)} \right) \tag{3}$$

where sf is the scale factor, R_L is the load resistor and offset (V) is 0 g value from a previous checkout.

4.3. Lessons learned

The cruise phase presents an important opportunity to verify accelerometry data in its various modes in a stable, zero-g, environment. This opportunity must be well exploited: for example, development of telecommands to allow the Servo to step through its all four measurement modes would have yielded useful information in terms of noise and better characterisation of the offset in each mode. Sensitive accelerometry measurements may also be useful in understanding any navigational/mission-related data. For example, the extra periodicity observed in Fig. 9 might have been useful in correlating any anomalous observations, although none has come to our attention in this instance.

An extremely useful feature would be to plan for and include controlled spacecraft rotations and a step-change to the rotation
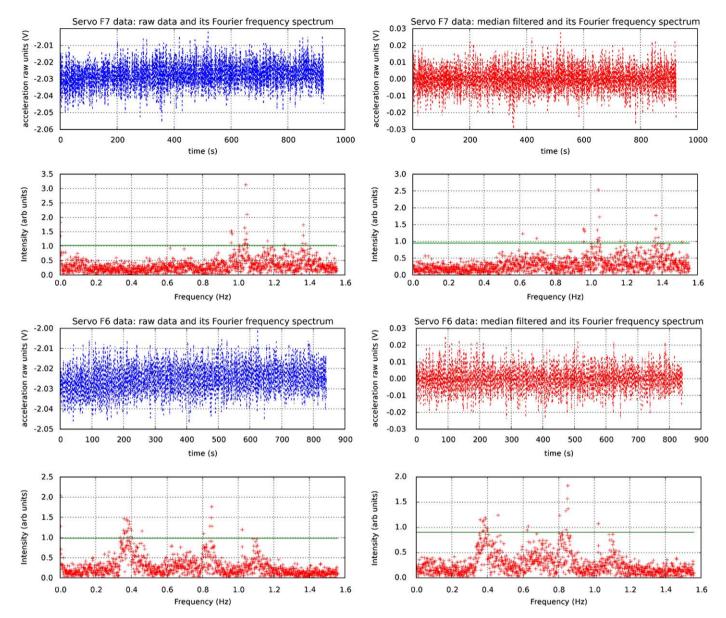
Fig. 9. Fourier analysis of F6 and F7 data. The top four plots represent the F7 checkout, while the bottom four plots relate to the F6 checkout. The F6 data shows dominant frequencies around 0.38 and 0.85 Hz; F7 has dominant components at around 1 (i.e. 0.96 and 1.04 Hz) and 1.37 Hz. Both spectra contain dominant frequency components not seen in a typical checkout, such as F16 data in Fig. 8. Without further spacecraft dynamics information, it is difficult to attribute the periodicity seen by the Servo in these particular checkouts. However, both of these checkouts coincide with the timeframe during which one of the spacecraft's reaction wheels was developing greater friction (and was later taken out of action). The checkouts also fall on either side of the closest Jupiter flyby (see text for dates).
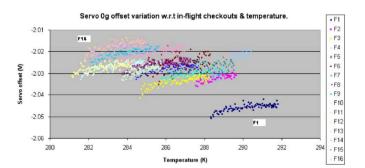

Fig. 10. Variation in the offsets from the high-resolution (up to ± 2 mg or $\sim \pm 0.02$ m s^{-2}) data from all cruise checkouts. These raw values must equate, on average, to zero acceleration. Hence, the cruise measurements are useful in obtaining the zero-g offset values (used in Eq. (2)). We see a small drift the Servo's offset 'upwards' on the plot over time (i.e. moving to less negative values).

rate during the time the accelerometer is 'on' in the cruise phase. While this might prove an undesirable addition from the navigation and space operations perspective, the output from such measurements will help verify calibration (of the scale factor) in-flight as well as monitor any changes in the sensitivity of the device.

5. Titan: entry, descent and landing (EDL)—data analysis

5.1. Early pre-entry/entry data

After its release from the Cassini orbiter on 25th December 2004, the Huygens probe coasted and encountered Titan's upper atmosphere on 14th January 2005 at an altitude of ~1500 km (Fulchignoni et al., 2005). Along with the various probe

parameters (Colombatti et al., 2008a), it is possible to estimate probe's spin rate at encounter from the most dominant frequency component (obtained by Fourier transform; see Fig. 12) from pre-encounter (or 'pre-entry') Servo data.

If the Servo was perfectly aligned with the probe's CM, then using the same technique as above (i.e. Fourier transform of early entry data) might yield information on atmospheric (or gravitational tidal) waves (Salby, 1996). Under appropriate conditions: i.e. (1) the probe must be spin-stabilised, (2) the Servo (or any other highly sensitive accelerometer) can only sense decelerations in the descent axis, and (3) group velocity of gravitational waves must be much smaller than probe's entry velocity ($<100\,\mathrm{cm\,s^{-1}}$ in Titan's case, (Strobel, 2006)) versus entry velocity of $\sim6\,\mathrm{km\,s^{-1}}$ (Atkinson et al., 2005), the chances of detecting such a tidal wave must improve.

5.2. Titan's atmospheric structure

The outputs of the Servo during the entry phase: Titan's upper atmosphere density, pressure and temperature profiles as a function of altitude (from 1500 to 160 km) have been presented in Fulchignoni et al. (2005) and are reproduced in Fig. 13. The density, ρ, in Eq. (4) is calculated from the probe's acceleration, a, its velocity relative to atmosphere, v (obtained by integrating a using the initial entry conditions), and the knowledge of probe's ballistic coefficient, $m/C_D \cdot A$ (where: m = probe's mass, C_D = drag coefficient, and A = probe's cross-sectional area).

$$\rho = \frac{2 \cdot m \cdot a}{C_D \cdot A \cdot v^2} \tag{4}$$

The pressure profile, P, is obtained by integrating the hydrostatic equilibrium: $\mathrm{d}P = -\rho \cdot g \cdot \mathrm{d}z$, where ρ = density, g = local gravity, and z = altitude. Finally, the temperature profile, T, is obtained from the ideal gas equation: $T = (P \cdot M_m)/(\rho \cdot k_B)$, where M_m = mean molecular mass and k_B = Boltzmann's constant.

The techniques used for determining the atmospheric profiles are described in more detail in Kazeminejad et al. (2007) and Withers et al. (2003, 2004). In general, the error on the profiles (in Fig. 13) is approximately 10%; mainly originating from the poor (time-correlated) knowledge of the angle of attack and velocity measurements that feed into the (estimated) probe's aerodynamic drag coefficient.

5.3. Descent under [stabiliser drogue] parachute

The Huygens parachute system consisted of two parachutes, a larger parachute (8.3 m diameter), known as the main parachute, was deployed for the first 15 min of the descent. The rest of the descent was on a smaller (3 m diameter), stabiliser drogue parachute. In this configuration, the probe was suspended by three bridle lines and a swivel mechanism to allow the probe to rotate (as shown in Fig. 14). Under the drogue parachute, there are two swing modes; a slower, 'rigid-pendulum' swing mode and a faster, 'half-scissors' swing mode. Parachute model during the descent phase gives oscillation frequency due to the faster swing mode at ~0.8 Hz, while the slower mode, with length of 12 m, at 0.05 Hz (i.e. period = 20 s) (Karkoschka et al., 2007).
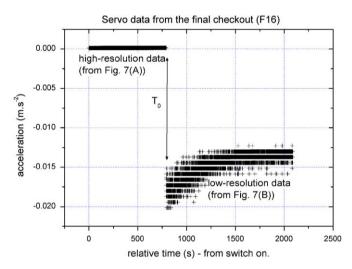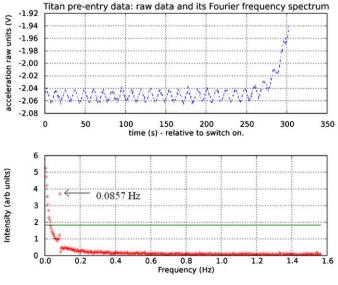

Fig. 11. When converted using the information from Appendix A, the high-resolution entry and the low-resolution descent data do not 'line-up' as they should given the constant (0 g) acceleration. This step in the two data sets from the same cruise checkout demonstrates the need to adjust the Servo's offset according to its measurement range as well as its operating time and temperature.
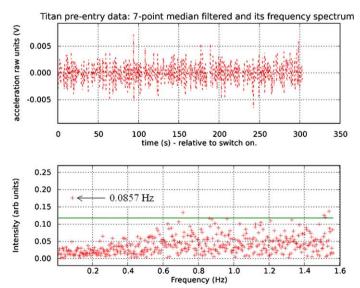

Fig. 12. Servo data prior to the atmosphere encounter and its frequency spectrum. The top-left figure shows atmosphere detection at the tail end of the plot. The dominant frequency component (at 0.086 Hz), along with other probe dynamics-related information, has been used to calculate the spin rate of ~7 rpm (Colombatti et al., 2008a).
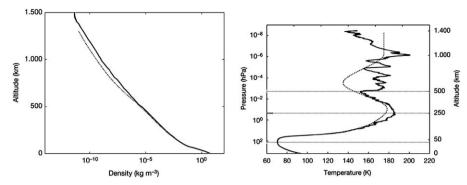
Fig. 13. Titan's upper atmosphere density (left), pressure and temperature (right) profiles were the main outputs of the Servo. These results were presented in Fulchignoni et al. (2005); all data above 150 km have been derived from the Servo's measurements of the Titan's atmosphere. The treatment of errors arising in deriving such atmospheric profiles from accelerometry measurements were first described in Peterson (1965b). An alternative method, described in Aboudan et al. (2008), uses 'extended Kalman filter' technique to derive the above results.
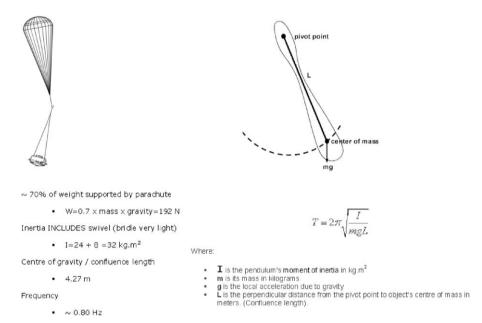

~ 70% of weight supported by parachute

- W=0.7 × mass × gravity=192 N

Inertia INCLUDES swivel (bridle very light)

- I=24 + 8 =32 kg.m^2

Centre of gravity / confluence length

- 4.27 m

Frequency

- ~ 0.80 Hz

$$T = 2\pi \sqrt{\frac{I}{mgL}}$$

Where:

- **I** is the pendulum's moment of inertia in kg.m^2
- **m** is its mass in kilograms
- **g** is the local acceleration due to gravity
- **L** is the perpendicular distance from the pivot point to object's centre of mass in meters. (Confluence length).

Fig. 14. Schematic of the Huygens probe under stabiliser chute (left), and the parachute model (right). Oscillations due to the faster 'half-scissors' swing mode should be around 0.8 Hz, while the slower 'rigid-pendulum' mode, with length of 12 m should be around 0.05 Hz (i.e. period = 20 s). The parachute calculations and details are available in Underwood et al. (2005).

The two plots in Fig. 15 (A and B) show the frequency components seen by the Servo; it is clear that the latter part of descent, from 62 to 48 km, only sees oscillations at 0.35 Hz: i.e. the 'half-scissors' model, predicting 0.8 Hz swings, is not valid in this region. The early part of the descent, from 86 to 62 km, sees oscillations on either side of the predicted 0.8 Hz, as well as (an equally dominant component) at 0.55 Hz.

5.4. Post-landing analysis

The Servo measurements were not telemetered between 1 km and landing in order to allocate maximum bandwidth to the 3-axes PZR accelerometers to detect the landing event. In post-landing configuration, the Servo measurements are shown in Fig. 16, where the bottom line (labeled 'Original') gives acceleration according to manufacturer's calibration (calculated using the values in Appendix A), and the top line (labeled 'Revised') gives the revised acceleration that is approximately 1% higher than in A. The 'Revised' acceleration values are calculated using Eq. (3), taking into account the zero-g offset seen during the

cruise phase (in Figs. 7(B) and 11, of approximately −0.010 V (or −0.015 m s^{-2})). An independent study by NASA Langley (NESC, 2007) also found the need for 1% upward revision in the Servo's acceleration measurements during their analysis.

5.5. Lessons learned

Aside from its science goals (i.e. determining atmospheric profiles), the accelerometry data from the mission phase can be useful in correlating other dynamic/engineering events such as buffeting and parachute behavior. In summary, the data can be a useful reference for many years after the mission.

6. Summary

The individual sections of this article address various development and data analysis phases that were encountered during the Huygens mission and should be applicable to other planetary missions involving an entry probe or a lander element. We hope
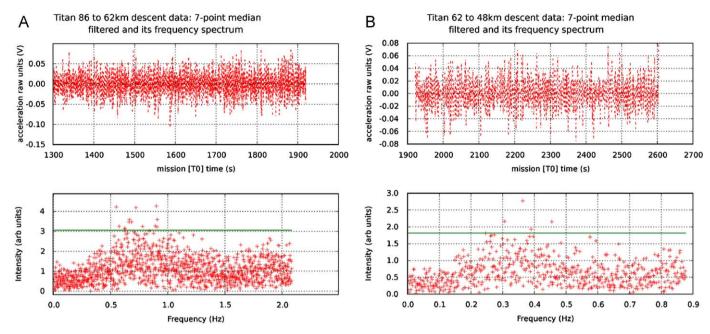
Fig. 15. (A) Frequency spectra from the probe's descent under the drogue parachute .While the descent from 86 to 62 km (Fig. 15(A)) show dominant frequency components around the modelled oscillation frequency of 0.8 Hz (in Fig. 14), the latter part of the descent: from 62 to 48 km (Fig. 15(B)), shows no evidence of the modelled frequency.
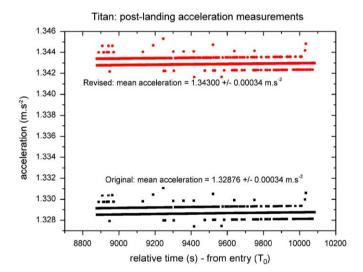

Fig. 16. Post-landing acceleration measurements (on Titan's surface) show the revised values to be higher by about 1% than original values. The revised value, calculated by taking the offset drift during cruise into account, is closer to the Titan's reference gravity of 1.345 m s^{-2}, quoted in Lebreton and Matson (2002).

this review article will serve as a useful reference for future accelerometry payloads and in planning for its data exploitation.

Since the Huygens mission was launched, there have been a number of missions to Mars; Beagle 2, Mars Exploration Rovers, Phoenix, and the Mars Science Laboratory (to be launched in September/October 2011)—all of which have/had accelerometry payloads. The challenges for larger future missions (leading possibly to a manned mission) to Mars are outlined in (Braun and Manning, 2006). The accelerometry data, along with the fast-growing ground tracking capability (Jones, 2004) will have a role to play on future missions, in the areas of EDL and atmospheric profiling. However, a common, 'off-the-shelf', accelerometry package for future missions remains elusive due to the large variations in the entry modules' requirements (especially in terms of mass, power, and size budgets allocated to accelerometry packages).

Appendix A. : Converting Servo data to acceleration (in m s^{-2}) from manufacturer's data

The equation for converting measurements from raw units (in V) to acceleration (in m s^{-2}) was given in Eq. (2) and can be re-written as

$$a(\text{m s}^{-2}) = \left(\frac{a(\text{V})}{R(\Omega)sf(\text{A/g})} - offset\,(\text{g}) \right)g \qquad (A1)$$

The manufacturer's calibration data (dated: January 1993) provide variation in the scale factor (sf (A/g)) and the offset ($offset$ (g)) as a function of temperature. From Figs. 17(A) and (B), the polynomial fits define the two parameters.

The polynomial fit gives the two parameters (in Eq. (A1)):

$$sf(\text{A/g}) = 1.30675\text{E} - 03 - 1.35046\text{E} - 07(T\,(\text{K})) + 4.02821\text{E}$$

$$-10(T\,(\text{K}))^2 offset(\text{g}) = -8.9642327\text{E} - 04 + 3.83652\text{E}$$

$$-06(T\,(\text{K})) - 0.00761\text{E} - 06(T\,(\text{K}))^2$$

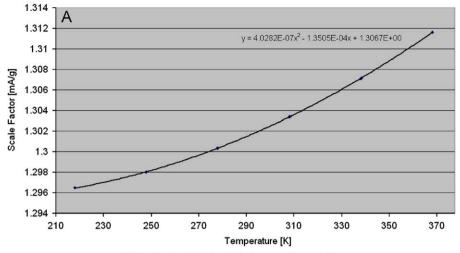where, g (in Eq. (A1)) is Earth's gravity $= 9.80708$ m s^{-2} (as provided by the manufacturer).

Servo's temperature measurements are converted from raw units (i.e. temperature in volts T (V)) to temperature (in K) using the relationship given in Eq. (A2):

$$T(\text{K}) = 109.23\,(T\,(\text{V}) - 2.5) \qquad (A2)$$

The appropriate value of the load resistance R in [Eq. (A1)] is selected by looking at the Servo settings in the HASI housekeeping

Manufacturer's data: Scale Factor versus Temperature

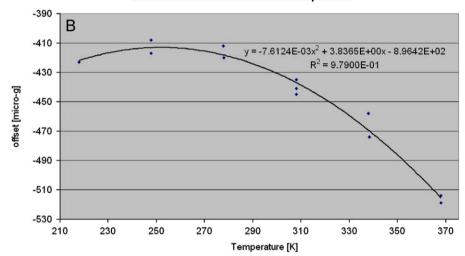**Manufacturer's data: offset versus Temperature**

Fig. 17. (A) Servo's scale factor as a function of temperature from manufacturer's calibration of the specific flight sensor. Changes to these values over time have not been monitored. (B): Servo's offset as a function of temperature from manufacturer's calibration of the specific flight sensor. These values can be monitored during cruise/ in-flight checkouts.

Table A1
Servo's load resistance values: for any measurement, the Servo will be in one of the four states above; a change in the state is reported in HASI's Housekeeping data.

Load resistance $R(\Omega)$	Gain	Resolution	Measurement range
453.00	Low	Low	$\pm 18.5\,g\ (=\pm 181.485\,\mathrm{m\,s^{-2}})$
4294.72	High	Low	$\pm 1.85\,g\ (=\pm 18.149\,\mathrm{m\,s^{-2}})$
411,109	Low	High	$\pm 20\,\mathrm{mg}\ (=\pm 0.196\,\mathrm{m\,s^{-2}})$
3,897,566	High	High	$\pm 2\,\mathrm{mg}\ (=\pm 0.0196\,\mathrm{ms^{-2}})$

data. In general, the early entry data fall into the 'high-gain, high-resolution' category in Table A1, whereas the post-landing acceleration measurements may be converted by using the 'high-gain, low-resolution' values.

References

Aboudan, A., Colombatti, G., Ferri, F., Angrilli, F., 2008. Huygens probe entry trajectory and attitude estimated simultaneously with Titan atmospheric structure by Kalman filtering. Planet. Space Sci. 56, 573–585.

Atkinson, D.H., Kazeminejad, B., Gaborit, V., Ferri, F., Lebreton, J.-P., 2005. Huygens probe entry and descent trajectory analysis and reconstruction techniques. Planet. Space Sci. 53, 586–593.

Braun, R.D., Manning, R.M., 2006. Mars exploration entry, descent and landing challenges, IEEEAC #0076, IEEE Aerospace Conference, Big Sky, MT.

Cancro, G.J., Tolson, R.H., Keating, G.M., 1998. Operational data reduction procedure for determining density and vertical structure of the Martian upper atmosphere from Mars global surveyor accelerometer measurements. NASA/CR-1998-208721.

Cardy, W., 1984. Q-Flex Accelerometer, Construction and Principle of Operation. Sundstrand Data Control Inc, TN -103.

Clausen, K.C., Hassan, H., Verdant, M., Couzin, P., Huttin, G., Brisson, M., Sollazzo, C., Lebreton, J.-P., 2002. The Huygens probe system design. Space Sci. Rev. 104, 155–189.

Colombatti G., et al., 2008a. Reconstruction of the trajectory of the Huygens probe using the Huygens atmospheric structure instrument (HASI). Planet. Space Sci. 56, 586–600.

Colombatti, G., Aboudan, A., Ferri, F., Angrilli, F., 2008b. Huygens probe entry dynamic model and accelerometer data analysis. Planet. Space Sci. 56, 601–612.

Fulchignoni, M., et al., 1997. The huygens atmospheric structure instrument. In: Huygens Science, Payload, and Mission, ESA SP-1177, pp. 163–176.

Fulchignoni, M., et al., 2002. The characterisation of Titan's atmospheric physical properties by the Huygens atmospheric structure instrument (HASI) Space Sci. Rev. 104, 395–431.

Fulchignoni, M., et al., 2005. In situ measurements of the physical characteristics of Titan's environment. Nature 438 785–791.

Gaborit, V., 2004. Procedure development for the trajectory reconstruction of a probe descending in a planetary atmosphere: application to Galileo and HASI balloon tests, ESA SP-544, pp. 151–162.

Hansen, C.J., Bolton, S.J., Matson, D.L., Spilker, L.J., Lebreton, J.-P., 2004. The Cassini–Huygens flyby of Jupiter. Icarus 172, 1–8.

Jones, D.L., 2004. Spacecraft tracking with the SKA. New Astro. Rev. 48, 1537–1542.

Jones, J.C., Giovagnoli, F., 1997. The Huygens Probe System Design. ESA SP-1177, pp. 25–45.

James, H.M., Nichols, N.B., Phillips, R.S., 1947. Theory of Servomechanisms. McGraw-Hill, New York, p. 133.

Karkoschka, E., Tomasko, M.G., Doose, L.R., See, C., McFarlane, E.A., Schroeder, S.E., Rizk, B., 2007. DISR imaging and the geometry of the descent of Huygens. Planet. Space Sci. 55, 1896–1935.

Kazeminejad, B., Perez-Ayucar, M., Lebreton, J.-P., Sanchez-Nogales, M., Bello-Mora, M., Strange, N., Roth, N., Popken, L., Clausen, K., Couzin, P., 2004. Simulation and analysis of the revised Huygens probe entry and descent trajectory and radio link modeling. Planet. Space Sci. 52, 799–814.

Kazeminejad, B., Atkinson, D.H., Pérez-Ayúcar, M., Lebreton, J.-P., Sollazzo, C., 2007. Huygens' entry and descent through Titan's atmosphere—methodology and results of the trajectory reconstruction. Planet. Space Sci. 55, 1845–1876.

Lebleu, D., Valentini, D., Schipper, A., 2005. Probe reference data for post flight analysis. Technical Note HUY.ASP.MIS.TN.0006, Alcatel Space.

Lebreton, J.-P., Matson, D.L., 2002. The Huygens probe: science, payload and mission overview. Space Sci. Rev. 104, 59–100.

Lebreton, J.-P., et al., 2005. An overview of the descent and landing of the Huygens probe on Titan. Nature 438 758–764.

Magalhães, J.A., Schofield, J.T., Seiff, A., 1999. Results of the Mars pathfinder atmospheric structure investigation. J. Geophys. Res. 104, 8943–8956.

NASA-TN-3770218, 1976. Entry Data Analysis for Viking Landers 1 and 2 Final report (NASA-CR-159388) by Martin Marietta Corp. (November 1976).

NESC, 2007. ITA of Cassini/Huygens probe entry, descent and landing (EDL) at Titan–Phase 2 Huygens probe reconstruction, NASA Engineering And Safety Center, Independent Technical Assessment/Inspection (ITA/I) Report, pp. 7–9.

Peterson, V.L., 1965a. A technique for determining planetary atmosphere structure from measured accelerations of an entry vehicle. NASA TN D-2669. Ames Research Center, California, USA.

Peterson, V.L., 1965b. Analysis of the errors associated with the determination of planetary atmosphere structure from measured accelerations of an entry vehicle. NASA-TR-R-225. Ames Research Center, California, USA.

Q-Flex Accelerometer Handbook, 1997. IHBK-101 11/97, AlliedSignal Inc.

Salby, M.L., 1996. Fundamentals of Atmospheric Physics. Academic Press, New York pp.440–478.

Seiff, A., 1963. Some possibilities for determining the characteristics of the atmospheres of Mars and Venus from gas-dynamic behaviour of a probe vehicle. NASA TN D-1770. Ames Research Center, California, USA.

Seiff, A., Knight, T.C.D., 1992. The Galileo probe atmosphere structure instrument. Space Sci. Rev. 60, 203–232.

Seiff, A., et al., 1997. The atmosphere structure and meteorology instrument on the Mars Pathfinder lander. J. Geophys. Res. 102, 4045–4056.

Strobel, D.F., 2006. Gravitational tidal waves in Titan's upper atmosphere. Icarus 182, 251–258.

The Electronics Handbook, 1996. CRCnetBASE, Jerry C. Whitaker, CRC press, pp 1840.

Underwood, J.C., Lingard, J.S., Neal, M.F., 2005. Huygens: Preliminary analysis of post-flight data. Prepared for Alcatel Space by Vorticity Ltd., Oxfordshire, UK.

Withers, P., Towner, M.C., Hathi, B., Zarnecki, J.C., 2003. Analysis of entry accelerometer data: a case study of Mars Pathfinder. Planet. Space Sci. 51, 541–561.

Withers, P., Towner, M.C., Hathi, B., Zarnecki, J.C., 2004. Review of the trajectory and atmospheric structure reconstruction for Mars Pathfinder. In: Planetary Probe Atmospheric Entry and Descent Trajectory Analysis and Science, ESA SP-544, pp. 163–174.

Zarnecki, J.C., Ferri, F., Hathi, B., Leese, M.R., Ball, A.J., Colombatti, G., Fulchignoni, M., 2004. In-flight performance of the HASI servo accelerometer and implications for results at Titan. In: Planetary Probe Atmospheric Entry and Descent Trajectory Analysis and Science, ESA SP-544, pp. 71–76.